ADVANCED FUNCTIONAL MATERIALS

Supporting Information

for *Adv. Funct. Mater.,* DOI: 10.1002/adfm.202108774

Transparent Refractory Aerogels for Efficient Spectral Control in High-Temperature Solar Power Generation

Zachary J. Berquist, Andrew J. Gayle, Neil P. Dasgupta, and Andrej Lenert**

Supplementary Information

Transparent Refractory Aerogels for Efficient Spectral Control in High-Temperature Solar Power Generation

Zachary J. Berquist,[1#]
Andrew J. Gayle,[2#]
Neil P. Dasgupta,[2,3*]
Andrej Lenert[1*]

[1] Department of Chemical Engineering, University of Michigan, Ann Arbor, MI 48109
[2] Department of Mechanical Engineering, University of Michigan, Ann Arbor, MI 48109
[3] Department of Materials Science and Engineering, University of Michigan, Ann Arbor, MI 48109

# These authors contributed equally
*E-mails: ndasgupt@umich.edu; alenert@umich.edu

Contents

1. Conformal and uniform alumina coating via ALD 2
2. Effect of a superficial coating 3
3. XRD of the refractory aerogel 4
4. Determination of the porosity and thermal conductivity 5
5. Atomic profiles after before and after aggressive aging 6
6. Effect of conformal ALD deposition on solar transmission 7
7. Effect of high-emissivity paint 8
8. Infrared absorption properties of the aerogels 9
9. RTE-HTE modeling 10
10. Review of high-temperature spectrally selective materials 11
11. Solar to electricity efficiency 12

Supplementary Note #1: Conformal and uniform alumina coating via ALD

We use the same ALD exposure recipe from our previous paper to deposit a uniform and conformal single-cycle layer of alumina on the aerogel monoliths.[1] ALD deposition of Al_2O_3 films on aerogels was performed in a custom hot-walled, cross-flow ALD reactor.[2] Trimethylaluminum (TMA, min. 97%, Sigma Aldrich) and deionized (DI) water were used as ALD precursors. Both precursors were kept at 37 °C, and the reactor temperature was maintained at 150 °C. In our exposure recipe, there are two steps in every cycle: exposure and purging. During the exposure step, the vacuum valve is closed, the Ar flow rate is reduced to 10 sccm, and the ALD precursor is pulsed into the chamber. We allow 400 s for the ALD precursors to diffuse into the aerogel monolith. For the purging step, the vacuum valve is reopened and the Ar flowrate is increased to 70 sccm. This step lasts 800 s.

Before depositing Al_2O_3, the aerogels were held at a vacuum pressure of 600 mTorr under constant Ar purging for at least 1 hour at 150 °C to ensure removal of excess water and other adsorbed species. We then performed 5 DI pre-cycles to saturate the aerogel monolith to ensure hydroxyl termination on the aerogel surface. We performed 12 TMA cycles and then 12 DI cycles. We show that we conformally coated the aerogel by using energy dispersive x-ray spectroscopy (EDX) to measure the atomic percentages of silicon, oxygen, and aluminum (Fig. S1).

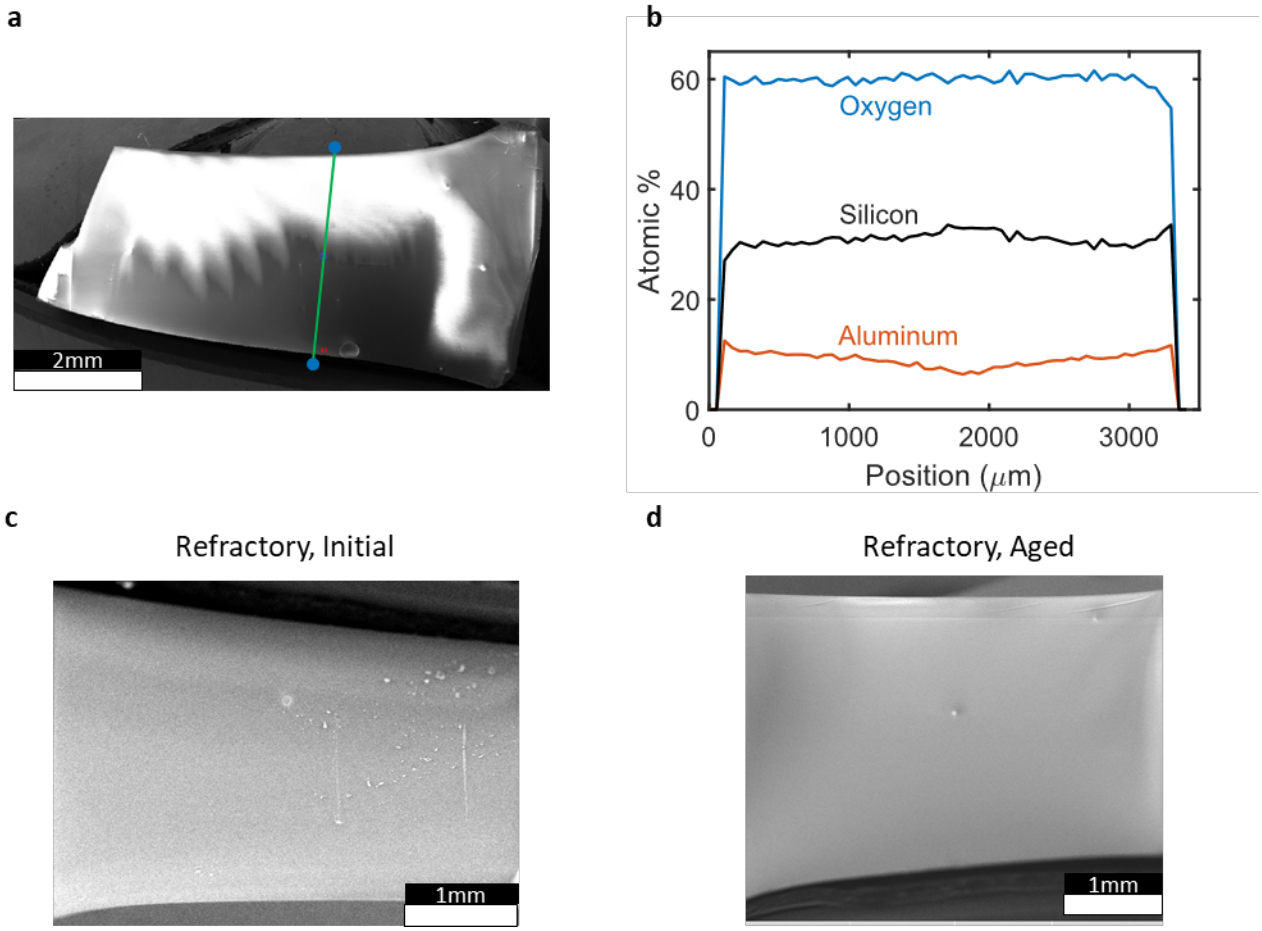


Figure S1. EDX spectroscopy. (a) Location of EDX scan with respect to the aerogel monolith. **(b)** Atomic percentages of silicon, oxygen, and aluminum on the refractory aerogel. **(c,d)** SEM images of the refractory aerogel before (c) and after (d) aging.

Supplementary Note #2: Effect of a superficial coating

When insufficient time is given for the ALD precursors to diffuse in and out of the porous aerogel, alumina builds up on the surface clogging pores and preventing a conformal coating. The superficial coating decreases solar transmission.

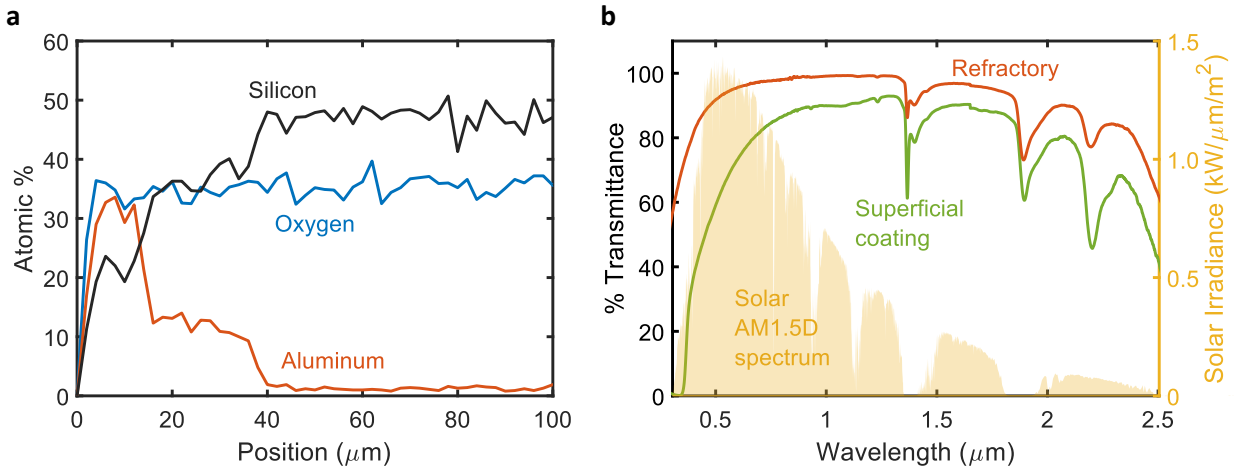


Figure S2. Effect of a superficial coating. (a) EDAX scan showing the buildup of alumina on the outer edges of the aerogel. **(b)** Solar transmittance of the superficially coated aerogel and the conformal refractory aerogel from the main text.

Supplementary Note #3: XRD of the refractory aerogel

X-ray diffraction spectroscopy (Fig. S3) confirms that both the silica and refractory aerogel are amorphous, even after aging.

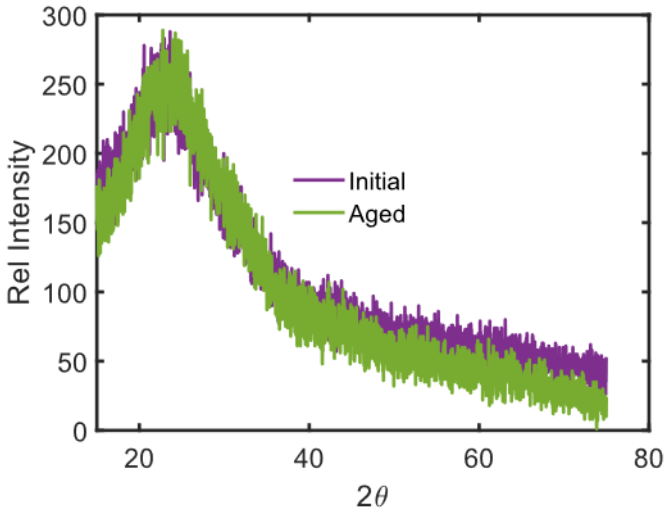


Figure S3. XRD of the refractory aerogel. The absence of sharp peaks confirms the material's amorphous structure.

Supplementary Note #4: Determination of the porosity and thermal conductivity

To calculate the porosity of the aerogels, we compute the volume of the solid network. We divide the relative mass components of each silica and alumina by their respective amorphous densities (2.2 and 3.0 g/cm^3, respectively). In our calculations, we use the mass of the aged aerogels because the initial aerogels contain significant amounts of water which will produce an artificially high density for the aerogels. For the refractory aerogels, the relative mass of alumina in the aerogels was calculated from the mass gained from the ALD process.

We recorded the room-temperature thermal conductivities with the transient plane source method using a commercial instrument (TPS, HotDisk) equipped with a thin spiral-resistor source/sensor (5465, HotDisk). The raw conductivities determined by the software were corrected using a polynomial correlation proposed by Zheng *et al*[3] for highly insulating samples.

Supplementary Note #5: EDAX line scans of aged aerogels

We measure the atomic percentage profile with respect to position for the aerogels both before and after aggressive aging (Figure S4). The atomic profiles remain unchanged within experimental error.

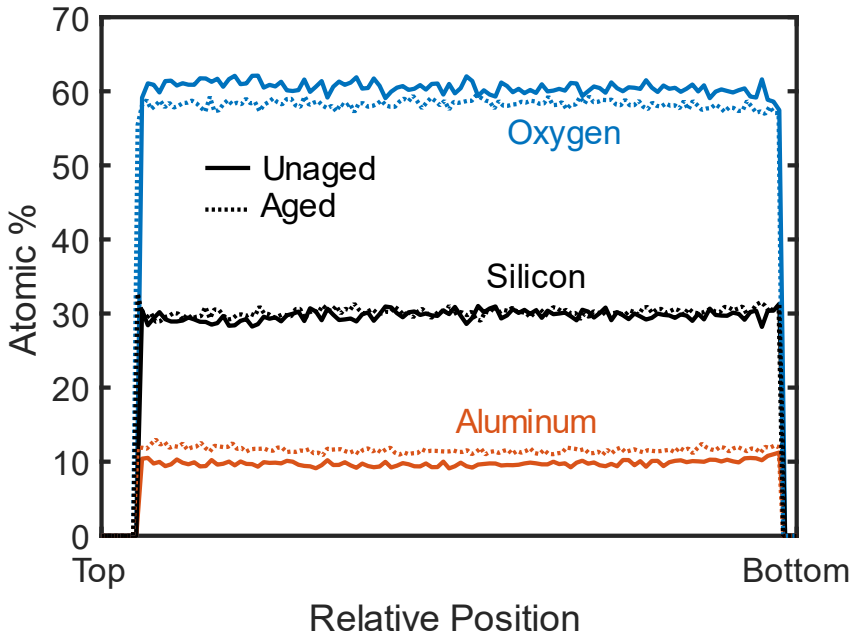


Figure S4. Atomic percentages from EDX line scans of the refractory aerogels before and after aging.

Supplementary Note #6: Effect of ALD deposition on solar transmission

The ALD coating decreases the total transmittance of the aerogel. Hemispherical reflectance data suggests the decrease in solar weighted transmittance (SWT) below 1200 nm is mainly due to scattering (Fig. S5). The increase in hemispherical reflectance indicates more back scattering from the refractory aerogel.

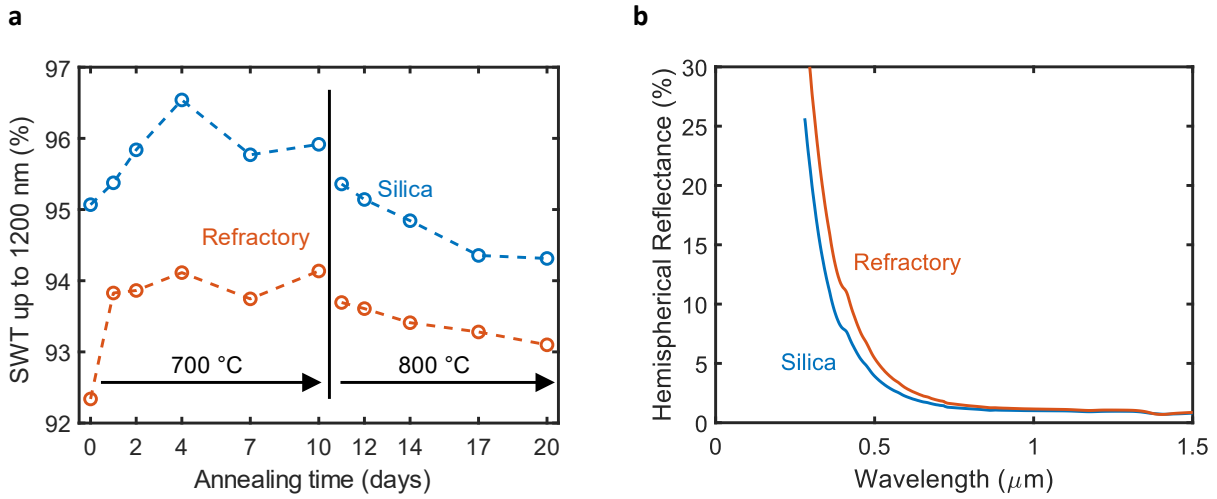


Figure S5. Solar weighted hemispherical transmittance and reflectance of aerogels below 1200 nm. The increase in hemispherical reflectance indicates the decrease in transmission is due to increased scattering. For wavelengths above 1000 nm, the attenuation is due to absorption as reflectance accounts for < 1%.

Supplementary Note #7: Effect of high-emissivity paint

We painted the SiC hot stage surface with a commercially available high-emissivity paint (Aremco HiE-Coat 840-CM). The heat flux through the aerogels was marginally different after painting because the aerogels are mostly opaque in the infrared. Thus, increasing the emissivity of the hot stage has a small effect on the overall heat losses.

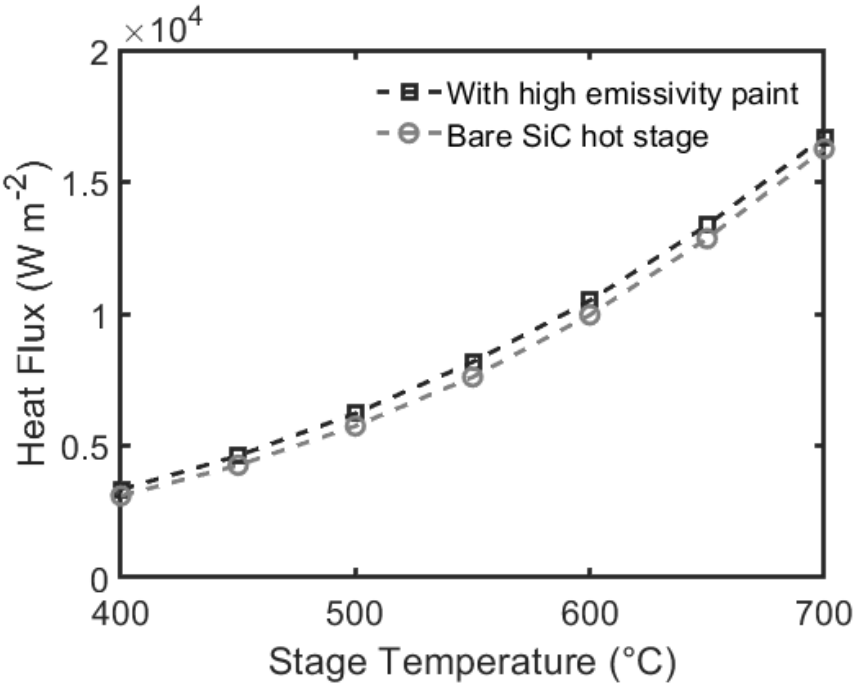


Figure S6. Comparison of aerogel heat losses with and without high emissivity paint.

Supplementary Note #8: Infrared absorption properties of the aerogels

Even after exposure to elevated temperatures, the refractory aerogels continue to be hydrophilic. After exposed to elevated temperatures, the refractory aerogels readily readsorb atmospheric water (Fig. S7a). Thermogravimetric analysis (TGA) further confirms this (Fig. S7b). Initially, the silica aerogel contains ~15% water by mass. After aging though, the mass change of the silica aerogel is effectively zero. As for the refractory, it still has ~5% mass in water weight after aging (initial refractory curve omitted for clarity).

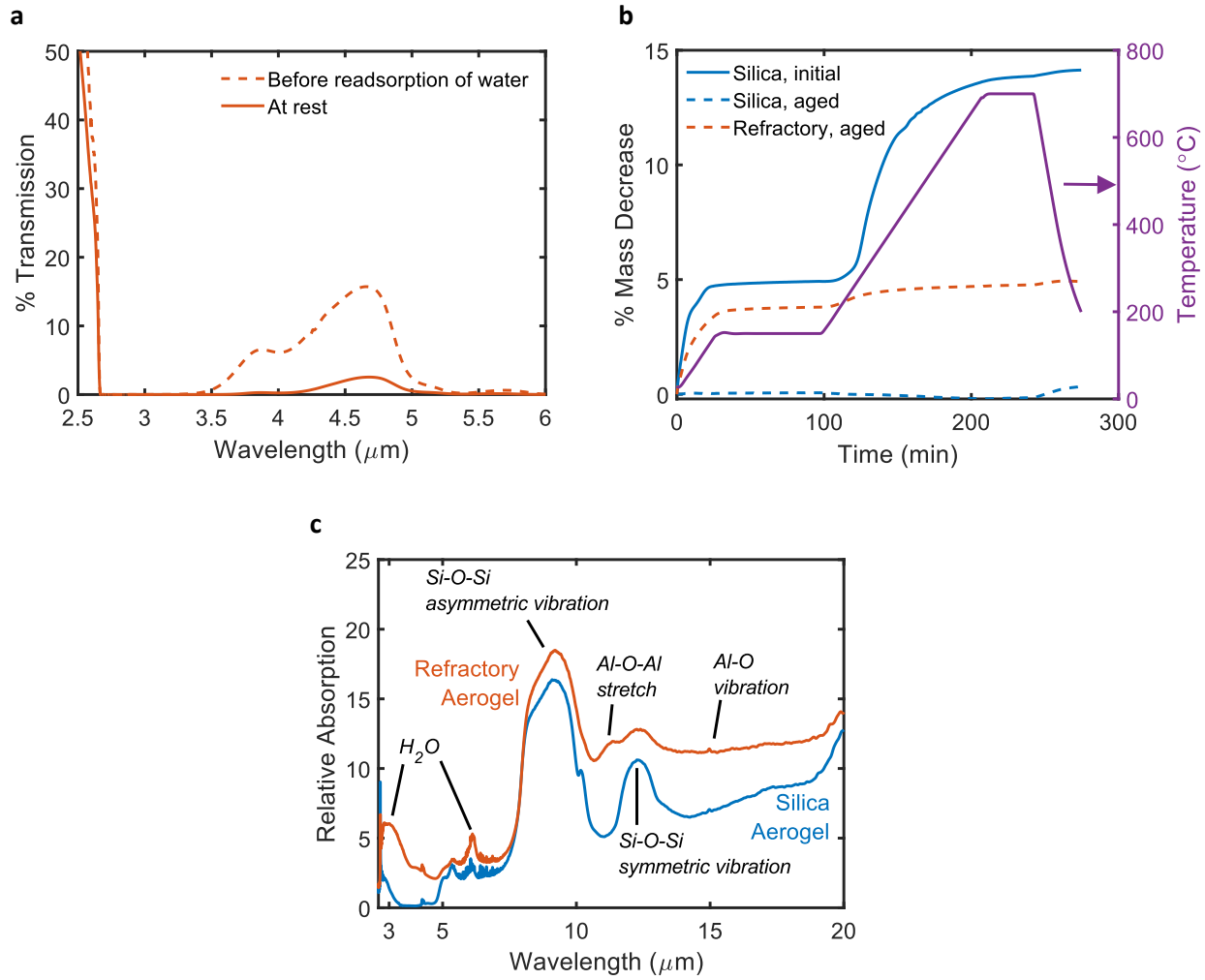


Figure S7. Hydrophilic nature of refractory aerogels. (a) Transmission between 3 – 5 μm increases during exposure to high temperatures as water is driven off the aerogel surface. However, it immediately begins to readsorb water and return to a state of large infrared attenuation. **(b)** TGA of silica and refractory aerogels of interest. **(c)** DRIFTS measurements of the aged aerogels.

Supplementary Note #9: RTE-HTE modeling

Both the heat transfer equation (HTE, Equation S1) and the radiative transfer equation (RTE, Equation S2) are required to accurately describe a system where conduction and radiation are important.

$$\nabla \cdot (k\nabla T) = \nabla \cdot q_r \tag{S1}$$

$$\frac{dI_\nu}{d\boldsymbol{s}} = -\beta_\nu I_\nu + (1-\sigma_\nu)\beta_\nu I_\nu + \frac{\beta_\nu \sigma_\nu}{4\pi}\int_{4\pi} I_\nu(\boldsymbol{s}_i)d\Omega_i \tag{S2}$$

The RTE is computationally expensive to solve since it is an integro-differential equation. To speed up the calculation, we split the thermal radiation spectrum into 12 bands and averaged the inputs for each band (Fig. S8). The scattering albedo, σ_ν, is the fraction of attenuation resulting from scattering. For wavelengths between 1 – 2 μm, we use a value of 0.5. Since scattering is negligible for wavelengths above 2 μm, we used a value of zero.[4] These values are consistent with previous literature.[5] A value of zero means all the attenuation is due to absorption. We choose 1 μm as the lower limit and 100 μm as the upper limit of our calculations because only 0.02% of the 700°C Planck's blackbody emission spectrum lies outside of this spectral range.

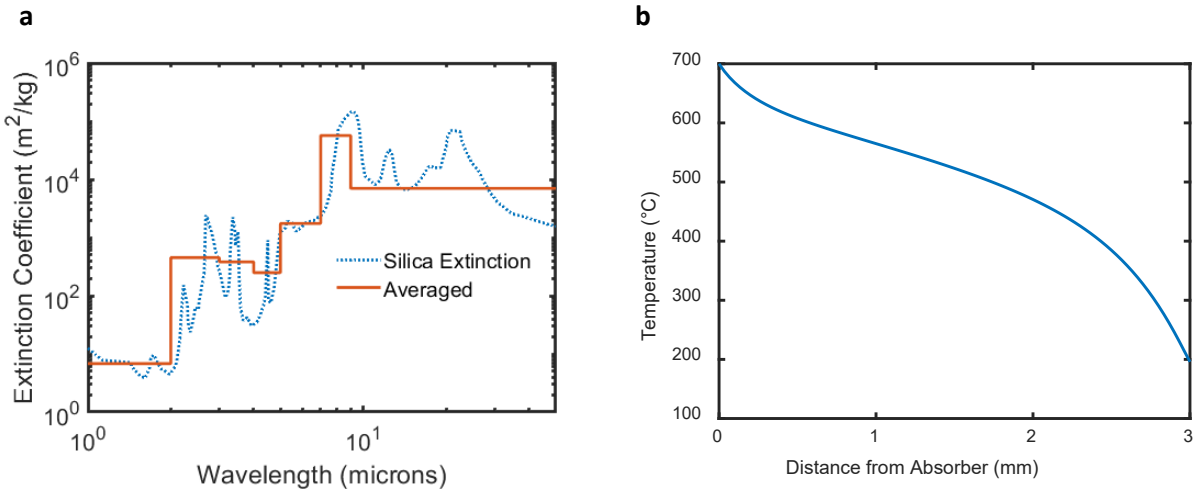


Figure S8. (a) Extinction coefficient of silica aerogels. The literature values (dashed blue line) and the averaged values for each band (orange line). **(b)** Simulated temperature profile of a silica aerogel on the 700 °C hot stage in vacuum.

Supplementary Note #10: Review of high-temperature spectrally selective materials

Despite its importance, selective absorbers and coatings are not commonly characterized at temperatures 500°C and above. To allow for comparison with other selective materials, we use the definition of spectral selectivity, $(\alpha_{eff}/\varepsilon_{eff})$, where α_{eff} is the effective solar absorptance and ε_{eff} is the effective emittance. For selective surfaces, α_{eff} and ε_{eff} are simply its solar absorptance and thermal emittance, respectively. For the refractory aerogel, α_{eff} is equal to its solar transparency since we assume the aerogel is used in tandem with a near-blackbody absorber. Lastly, ε_{eff} for the refractory aerogels is computed from the following relation: $\varepsilon_{eff} = Q_{loss}/Q_{BB}$ where Q_{loss} is the experimental heat loss value and Q_{BB} is the emissive power of blackbody at the corresponding temperature.

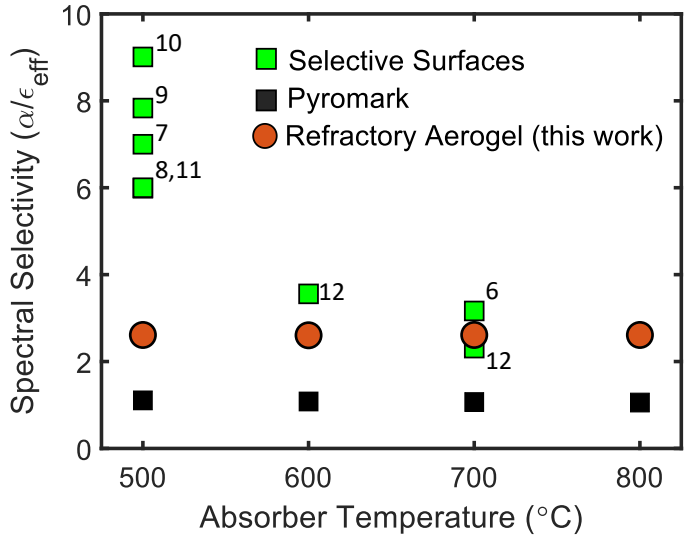


Figure S9. Spectral selectivity of high temperature selective materials.

Supplementary Note #11: Solar to electricity efficiency

Current CSP plants operate steam Rankine cycles at ~400°C which have a heat-to-electrical efficiency (η_{cycle}) of approximately 31% while supercritical CO_2 cycles at 700°C have an efficiency of ~47%.[13] Additionally, state-of-the-art selective surfaces (SS) have a receiver efficiency ($\eta_{receiver}$) of about 84% at 400°C.[5] Neglecting any additional losses from operating at higher temperatures, the receiver-side efficiency (RSE) of a supercritical CO_2 power cycle with a refractory aerogel (RA) is ~36% compared to ~26% for current steam Rankine cycles with selective surfaces (Equation S3).

$$RSE = \eta_{receiver} * \eta_{cycle} \tag{S3}$$

$$RSE(SS, steam, 400°C) = \eta_{receiver}(SS, 400°C) * \eta_{cycle}(400°C)$$
$$\boldsymbol{RSE_{400°C} = (0.84) * (0.31) = 26\%}$$

$$RSE(RA, sCO_2, 700°C) = \eta_{receiver}(RA, 700°C) * \eta_{cycle}(700°C)$$
$$\boldsymbol{RSE_{700°C} = (0.77) * (0.47) = 36\%}$$

References

(1) Gayle, A. J.; Berquist, Z. J.; Chen, Y.; Hill, A. J.; Hoffman, J. Y.; Ashley, R.; Lenert, A.; Dasgupta, N. P. Tunable Atomic Layer Deposition into Ultra-High-Aspect-Ratio (> 60 , 000 : 1) Aerogel Monoliths Enabled by Transport Modeling. *Chem. Mater.* **2021**, No. 33.

(2) Dasgupta, N. P.; Mack, J. F.; Langston, M. C.; Bousetta, A.; Prinz, F. B. Design of an Atomic Layer Deposition Reactor for Hydrogen Sulfide Compatibility. *Rev. Sci. Instrum.* **2010**, *81* (4), 044102.

(3) Zheng, Q.; Kaur, S.; Dames, C.; Prasher, R. S. Analysis and Improvement of the Hot Disk Transient Plane Source Method for Low Thermal Conductivity Materials. *Int. J. Heat Mass Transf.* **2020**, *151*.

(4) Zhao, L.; Yang, S.; Bhatia, B.; Strobach, E.; Wang, E. N. Modeling Silica Aerogel Optical Performance by Determining Its Radiative Properties. *AIP Adv.* **2016**, *6* (2).

(5) McEnaney, K.; Weinstein, L.; Kraemer, D.; Ghasemi, H.; Chen, G. Aerogel-Based Solar Thermal Receivers. *Nano Energy* **2017**, *40* (July), 180–186.

(6) Rinnerbauer, V.; Lenert, A.; Bierman, D. M.; Yeng, Y. X.; Chan, W. R.; Geil, R. D.; Senkevich, J. J.; Joannopoulos, J. D.; Wang, E. N.; Soljačič, M.; Celanovic, I. Metallic Photonic Crystal Absorber-Emitter for Efficient Spectral Control in High-Temperature Solar Thermophotovoltaics. *Adv. Energy Mater.* **2014**, *4* (12), 1–10.

(7) Cao, F.; Kraemer, D.; Tang, L.; Li, Y.; Litvinchuk, A. P.; Bao, J.; Chen, G.; Ren, Z. A High-Performance Spectrally-Selective Solar Absorber Based on a Yttria-Stabilized Zirconia Cermet with High-Temperature Stability. *Energy Environ. Sci.* **2015**, *8* (10), 3040–3048.

(8) Cao, F.; Kraemer, D.; Sun, T.; Lan, Y.; Chen, G.; Ren, Z. Enhanced Thermal Stability of W-Ni-Al2O3 Cermet-Based Spectrally Selective Solar Absorbers with Tungsten Infrared Reflectors. *Adv. Energy Mater.* **2015**, *5* (2), 1–7.

(9) Ning, Y.; Wang, W.; Wang, L.; Sun, Y.; Song, P.; Man, H.; Zhang, Y.; Dai, B.; Zhang, J.; Wang, C.; Zhang, Y.; Zhao, S.; Tomasella, E.; Bousquet, A.; Cellier, J. Optical Simulation and Preparation of Novel Mo/ZrSiN/ZrSiON/SiO2 Solar Selective Absorbing Coating. *Sol. Energy Mater. Sol. Cells* **2017**, *167* (March), 178–183.

(10) Wang, X.; Gao, J.; Hu, H.; Zhang, H.; Liang, L.; Javaid, K.; Zhuge, F.; Cao, H.; Wang, L. High-Temperature Tolerance in WTi-Al2O3 Cermet-Based Solar Selective Absorbing Coatings with Low Thermal Emissivity. *Nano Energy* **2017**, *37* (April), 232–241.

(11) Li, Y.; Lin, C.; Zhou, D.; An, Y.; Li, D.; Chi, C.; Huang, H.; Yang, S.; Tso, C. Y.; Chao, C. Y. H.; Huang, B. Scalable All-Ceramic Nanofilms as Highly Efficient and Thermally Stable Selective Solar Absorbers. *Nano Energy* **2019**, *64* (July).

(12) Wang, H.; Alshehri, H.; Su, H.; Wang, L. Design, Fabrication and Optical Characterizations of Large-Area Lithography-Free Ultrathin Multilayer Selective Solar Coatings with Excellent Thermal Stability in Air. *Sol. Energy Mater. Sol. Cells* **2018**, *174* (June 2017), 445–452.

(13) Weinstein, L. A.; Loomis, J.; Bhatia, B.; Bierman, D. M.; Wang, E. N.; Chen, G. Concentrating Solar Power. *Chem. Rev.* **2015**, *115* (23), 12797–12838.